Published in final edited form as:
Dev Cell. 2014 May 27; 29(4): 377–391. doi:10.1016/j.devcel.2014.04.022.

APC^{Cdc20} Suppresses Apoptosis through Targeting Bim for Ubiquitination and Destruction

Lixin Wan[1], **Mingjia Tan**[2], **Jie Yang**[2,3], **Hiroyuki Inuzuka**[1], **Xiangpeng Dai**[1], **Tao Wu**[4], **Jia Liu**[1,5], **Shavali Shaik**[1], **Guoan Chen**[6], **Jing Deng**[7], **Marcos Malumbres**[8], **Anthony Letai**[7], **Marc W. Kirschner**[4], **Yi Sun**[2], and **Wenyi Wei**[1,9]

[1]Department of Pathology, Beth Israel Deaconess Medical Center, Harvard Medical School, Boston, MA 02215, USA

[2]Department of Radiation Oncology, University of Michigan, Ann Arbor, MI 48109, USA

[3]Department of Biochemistry and Molecular Cell Biology, Shanghai Key laboratory for tumor microenvironment and inflammation, Shanghai Jiaotong University School of Medicine, Chongqing Road, Shanghai 200025, P. R. China

[4]Department of Systems Biology, Harvard Medical School, Boston, MA 02115, USA

[5]Institute of Mitochondrial Biology and Medicine, School of Life Science and Technology, Xi'an Jiaotong University, Xi'an, Shaanxi 710049, P. R. China

[6]Thoracic Surgery, University of Michigan, Ann Arbor, MI 48109, USA

[7]Department of Medical Oncology, Dana-Farber Cancer Institute, Boston, MA 02215, USA

[8]Cell Division and Cancer group, Spanish National Cancer Research Centre (CNIO), Madrid 28029, Spain

SUMMARY

APC^{Cdc20} plays pivotal roles in governing mitotic progression. By suppressing APC^{Cdc20}, anti-mitotic agents activate the spindle-assembly-checkpoint (SAC), and induce apoptosis after prolonged-treatment, while depletion of endogenous Cdc20 suppresses *in vivo* tumorigenesis in part by triggering mitotic arrest and subsequent apoptosis. However, the molecular mechanism(s) underlying apoptosis induced by Cdc20 abrogation remains poorly understood. Here we report that the BH3-only pro-apoptotic protein Bim is an APC^{Cdc20} target, as such depletion of Cdc20 sensitizes cells to apoptotic stimuli. Strikingly, Cdc20 and multiple APC-core components were identified in an siRNA screen that upon knockdown sensitizes otherwise resistant cancer cells to chemo-radiation therapies in a Bim-dependent manner. Consistently, human Adult-T-cell-

[9]To whom correspondence should be addressed: wwei2@bidmc.harvard.edu.

SUPPLEMENTAL INFORMATION

Supplemental Information includes seven supplemental figures and supplemental experimental procedures can be found with this article online.

Leukemia (ATL) cells that acquire elevated APC^{Cdc20} activity via expressing the Tax-viral-oncoprotein, exhibit reduced Bim levels and resistance to anti-cancer agents. These results reveal an important role for APC^{Cdc20} in governing apoptosis, strengthening the rationale for developing specific Cdc20 inhibitors as effective anti-cancer agents.

INTRODUCTION

The Anaphase Promoting Complex (APC) plays critical roles in regulating timely cell cycle progression in both the M and G1 phases (King et al., 19f96). In doing so, the APC core forms two functionally distinct E3 ubiquitin ligase sub-complexes, APC^{Cdc20} and APC^{Cdh1}, by associating with the substrate-recruiting proteins, Cdc20 and Cdh1, respectively. APC^{Cdc20} plays an indispensable role during the metaphase to anaphase transition as well as mitotic exit by targeting various key cell cycle regulators including Securin and Cyclin B for ubiquitin-mediated destruction (Hagting et al., 2002). Previous studies have revealed a central role for suppressing APC^{Cdc20} in the establishment and maintenance of the spindle assembly checkpoint (SAC) (Reddy et al., 2007). Although Bim (Bouillet et al., 1999; Tan et al., 2005) and Mcl-1 (Inuzuka et al., 2011; Wertz et al., 2011) have been implicated in apoptosis induced by anti-mitotic as well as DNA damage agents, it remains elusive whether there is a causal relationship between the inactivation of APC^{Cdc20} and cellular apoptotic responses. More importantly, many tumor-derived cell lines exhibit slippage from G2/M arrest to escape cell death induced by anti-cancer agents that activate the SAC (Gascoigne and Taylor, 2008). Hence, a further mechanistic understanding of how inhibition of APC^{Cdc20} induces apoptosis would benefit the design of more effective anti-cancer agents.

In support of the notion that inhibition of APC^{Cdc20} activity leads to induction of apoptosis, a recent study demonstrated that genetic ablation of endogenous Cdc20 could block *in vivo* tumorigenesis in a skin-tumor mouse model, largely due to elevated cellular apoptosis (Manchado et al., 2010). In concert with this finding, depleting endogenous Cdc20, which is frequently overexpressed in various cancer cell lines (Kidokoro et al., 2008), led to mitotic arrest followed by cell death (Huang et al., 2009). Consistently, Cdc20 was found to be highly expressed in various types of human tumors (Jiang et al., 2011; Kato et al., 2012). These findings advocate for elevated Cdc20 expression as a possible prognostic marker and therapeutic target in treating various human cancers. Indeed, inactivating APC by an Ile-Arg(IR)-tail-mimetic, pro-TAME, which inhibits both APC^{Cdc20} and APC^{Cdh1}, also induced cell death in multiple cancer cell lines (Zeng et al., 2010). However, it remains unclear mechanistically how inhibiting APC^{Cdc20} provokes cellular apoptosis. These studies prompted us to further explore the downstream signaling molecules that trigger the apoptotic responses following inhibition of APC^{Cdc20}. We report here that the pro-apoptotic protein Bim is a ubiquitin substrate of APC^{Cdc20} and that Bim accumulation upon APC^{Cdc20} knockdown contributes to apoptosis induction and chemo-radiation sensitization.

RESULTS

Bim abundance is reduced during mitosis when APC^{Cdc20} is most active

As APC^{Cdc20} functions as an E3 ubiquitin ligase, we started our investigation by examining whether any of the various key apoptotic regulators with pro-apoptotic (such as BH3-only proteins) or anti-apoptotic (such as Bcl-2 homologues) properties is a potential APC^{Cdc20} substrate. We primarily focused on the BH3-only family of proteins because of their prominent roles in triggering apoptotic responses (Youle and Strasser, 2008). Notably, the expression levels of most BH3-only proteins we examined did not significantly fluctuate during the cell cycle except Bim, which displayed a dramatic reduction in M phase, when APC^{Cdc20} is most active (Figures 1A and 1B). Moreover, a sharp decrease in protein abundance during M phase was similarly observed for well-characterized APC^{Cdc20} substrates including p21 (Amador et al., 2007) and Securin (Yu, 2007), indicating that Bim might be a possible APC^{Cdc20} substrate. Consistently, an inverse correlation between APC^{Cdc20} activity and the abundance of Bim was also observed in U2OS and T98G cells synchronized by double thymidine block (Figures 1C and 1D).

Previous results have demonstrated that in baby mouse kidney epithelial cells (BMK) (Tan et al., 2005), Bim abundance was upregulated by anti-mitotic drugs such as Taxol, which activates SAC to suppress APC^{Cdc20} (Fang et al., 1998). Consistently, accumulation of Bim was also observed in non-transformed cells including mouse embryonic fibroblasts (MEFs) (Figures 1E and S1A), NIH-3T3 (Figure S1B) and immortalized human fibroblasts (Figure S1C) treated with Taxol or Nocodazole. However, Bim upregulation was not observed after Taxol treatment in transformed human cancer cell lines we examined (Figure S1D). This might be in part due to frequent activation of Ras/ERK/RSK signaling pathways in human cancers (Tan et al., 2005), which governs Bim ubiquitination in a $SCF^{\beta\text{-}TRCP}$-dependent manner (Dehan et al., 2009). Consistent with a previous report (Nilsson et al., 2008), Cdc20 levels were significantly reduced after prolonged-mitotic arrest (Figure 1E), which may be in part due to elevated Cdc20 self-ubiquitination that could not be completely blocked by the MAD2 inhibitory complex (Reddy et al., 2007). More interestingly, in keeping with a critical role for Bim in DNA damage responses (Happo et al., 2010), various DNA damaging agents also resulted in elevated Bim abundance in part by reducing Cdc20 abundance via yet unknown mechanism(s) (Figure 1F).

Cdc20 deficiency leads to Bim upregulation

To further investigate the causal link between Cdc20 activity and Bim protein abundance, we depleted endogenous Cdc20 by multiple independent shRNAs in various cell lines, and found that Cdc20 knockdown led to a significant upregulation of Bim, but not other BH3-only proteins (Figures 2A and 2B; S2A and S2B). Furthermore, as observed previously (Dehan et al., 2009), depletion of endogenous β-TRCP also resulted in an upregulation of Bim (Figure 2C and S2C), suggesting that similar to many important cellular regulators including p53 (Brooks and Gu, 2011) and c-Jun (Wei and Kaelin, 2011), Bim stability might be regulated by multiple ubiquitin E3 ligases (Figure S3C). Although depletion of Cdh1 also led to elevated Bim expression (Figures 2B, 2C and S2B), depletion of Cdc20 in HCT116 (Figure 2B), HeLa (Figure S2B) or UMSCC-12 (Figures 7B and S7E) cells led to a more

dramatic Bim accumulation. Furthermore, Bim expression was more significantly reduced during M phase when APC^{Cdc20} activity is high (Figures 1A, 1C and 1D) and anti-mitotic agents primarily activate SAC to suppress APC^{Cdc20} (Figure 1E) (Yu, 2007), in the following studies we chose to focus primarily on characterizing Bim as a physiological ubiquitin substrate for APC^{Cdc20}.

To gain further mechanistic insights into the physiological role of Cdc20 in modulating Bim abundance, we generated HCT116 and immortalized primary human foreskin fibroblasts expressing a Tet-on inducible shCdc20. Notably, in both cell lines, Bim was upregulated after doxycycline-induced Cdc20 depletion (Figures 2D and S2D). Conversely, doxycycline-induced ectopic expression of Cdc20 in HCT116 cells led to a marked reduction of Bim levels and other known Cdc20 substrates (Figure 2E). More importantly, re-introducing WT- but not an E3 ligase-deficient N-terminal fragment of Cdc20 (Reimann et al., 2001), into Cdc20-depleted human foreskin fibroblasts reduced Bim levels comparable to shGFP-infected cells (Figures 2F and 2G), further supporting for a causal relationship between Cdc20 depletion and Bim accumulation.

In further support of a physiological role for Cdc20 in governing Bim stability, acute deletion of Cdc20 in MEFs (Manchado et al., 2010) led to elevated expression of Bim, but not other BH3-only proteins Puma or Bid (Figure 2H). Furthermore, an elevation of Bim was observed in cells treated with the pan-APC inhibitor pro-TAME (Zeng et al., 2010) (Figure 2I), or the 26S proteasome inhibitor MG132 (Figure 2J). More importantly, the increase in Bim abundance following Cdc20 depletion is largely due to an increased Bim half-life (Figures S2F and S2G), with minimal changes in Bim mRNA levels (Figures S2H and S2I), indicating that Cdc20 might mainly regulate Bim levels through a posttranslational mechanism.

It is critical to note that in most experimental conditions where Cdc20 was depleted or inactivated, we routinely treated cells with the caspase inhibitor, N-benzyloxycarbonyl-Val-Ala-Asp-fluoromethylketone (z-VAD-fmk) (Hara et al., 1997), before harvesting to prevent cell death induced by Bim upregulation. On the other hand, to further elucidate the role of Bim in apoptosis induced by Cdc20-deficiency, we used siRNA oligos to deplete Cdc20 in multiple cell lines and found that accompanied with Bim accumulation, Cdc20-depleted cells displayed a dramatic increase in apoptotic cells (Figures 2K, 2L and S2J). More importantly, Cdc20 depletion-induced apoptosis was largely compromised after additional depletion of endogenous Bim (Figures 2M–O, S2K–M). In support of the critical role for Bim in Cdc20 knockdown-induced apoptosis, when control and Bim-depleted $Cdc20^{lox/lox}/RERT^{+/Cre}$ MEFs (Figure S2N) were treated with 4-Hydroxytamoxifen (4-OHT) to induce Cre-mediated Cdc20 depletion, there was a delay of the onset of apoptosis (Figure S2O). Additionally, $Bak^{-/-}/Bax^{-/-}$ MEFs were resistant to Cdc20 depletion (Figure S2P) and Taxol induced apoptosis (Figure S2Q), further demonstrating that Cdc20 deficiency induced cell death through the mitochondrial apoptosis pathway, in which Bim plays an indispensable role (Gross et al., 1999). Therefore, these results coherently indicate a critical role for Bim in apoptotic response triggered by Cdc20 deficiency.

Bim is stabilized in Cdc20-depleted M phase cells

Importantly, depletion of Cdc20 significantly stabilized Bim in M phase, resulting in a rather nonfluctuation pattern of Bim expression across the cell cycle (Figures 3A, 3B and S3A). Interestingly, a significant stabilization of p21, another reported substrate of Cdc20, but not Cdh1 (Amador et al., 2007), in M phase was also observed upon depletion of Cdc20. We also noticed that Bim levels decreased in late S phase, where Cdc20 is largely inactive (Figures 3A and S3A), indicating that E3 ligase(s) other than Cdc20 might contribute to Bim regulation (Figure S3C). Consistent with this notion, Bim is stabilized in S, but not M phase when β-TRCP was depleted in T98G cells (Figure S3A). However, Bim was stabilized even in late S phase after depleting Cdc20 (Figure S3A). Given that we also observed a reduction in both p-ERK and p-RSK in Cdc20-depleted cells, we speculate that during S phase depleting Cdc20 might indirectly inhibit $SCF^{\beta\text{-}TRCP}$-mediated ubiquitination of Bim that requires phosphorylation of Bim by ERK/RSK (Dehan et al., 2009).

Consistent with an upregulation of Bim, Cdc20-depleted cells displayed more sub-G1 DNA content and cleaved-Caspase 3 compared with control cells (Figures 3A and 3B), indicating increased cell death after depletion of Cdc20. Stabilization of Bim in M phase and early G1 phase was also observed in shCdc20-HeLa cells (Figures 3C and 3D) or U2OS cells (Figure S3B). Importantly, although depletion of β-TRCP also led to a significant induction of Bim expression, this occurred in late G1/S phase (4–6 hours post-Nocodozole release) and no obvious elevation of Bim was observed in M and early G1 phases (0–2 hours post-Nocodozole release) (Figures 3C and 3D). On the other hand, depletion of Cdc20 mainly led to an upregulation of Bim in M and early G1 phases (0–2 hours), as well as in 4–6 hour post-Nocodazole release in part due to a delayed mitotic exit (Figures 3C and 3D). Therefore, these results suggested that both APC^{Cdc20} and $SCF^{\beta\text{-}TRCP}$ are upstream E3 ligases for Bim, which may exert their critical regulatory functions towards Bim in different cell cycle phases, or in response to different upstream signal(s) (Figure S3C). A similar mechanism has been previously reported for regulation of p21 stability by both APC and SCF in different cell cycle phases (Amador et al., 2007).

Cdc20 specifically interacts with Bim through its C-terminal WD40 repeats motif

In support of Bim being a putative Cdc20 substrate, Bim specifically interacted with the WD40-repeats domain of Cdc20 (Figures 4A and 4B), through which Cdc20 recruits substrates to the APC core complex (Yu, 2007). Consistently, purified recombinant GST-Bim only interacts *in vitro* with full length and WD40 domain, but not N-terminal Cdc20 (Figures 4C–E). Furthermore, endogenous Bim was detected to co-immunoprecipitate with endogenous Cdc20 and the APC core subunit Cdc27 (Figure 4F), strengthening the physiological role of Cdc20 in modulating Bim stability.

More importantly, GST-Bim only specifically interacted with Cdh1 and Cdc20, but not Skp2, or other F-box proteins containing the WD40-repeats domain examined (Figure 4G). Notably, interaction between β-TRCP1 and GST-Bim was only observed after ERK and RSK-mediated phosphorylation of GST-Bim (Figure S4A) (Dehan et al., 2009). On the other hand, interaction between Cdc20 and GST-Bim was not affected by ERK and RSK-mediated phosphorylation (Figure S4B). These results confirmed that unlike β-TRCP

(Dehan et al., 2009), phosphorylation of Bim by ERK/RSK is not required for Cdc20 to interact with Bim.

Cdc20 promotes Bim ubiquitination and subsequent degradation in a D-box-dependent manner

We found that BimEL contains two evolutionarily conserved D-boxes (Figures 5A and 5B) (Harper et al., 2002). More importantly, deletion of these two putative D-boxes (named ΔD1D2-Bim) disrupted Cdc20-mediated destruction of Bim *in vivo* (Figures 5C and 5D), or destruction of Bim *in vitro* by purified HeLa M-phase extracts containing active APC^{Cdc20} (Wu et al., 2010) (Figures 5E and 5F). Moreover, compared with WT-Bim, ectopically expressed ΔD1D2-Bim was stabilized in HeLa cells released from Nocodazole arrest (Figure 5G), indicating that deletion of two D-boxes allowed Bim to escape Cdc20-mediated destruction in M phase. Consistently, ΔD1D2-Bim failed to interact with Cdc20 *in vivo* (Figure 5H) and *in vitro* (Figures 5I–J and S5A–C). Moreover, deletion of these two D-boxes also significantly affected APC^{Cdc20}-mediated poly-ubiquitination of Bim both *in vivo* (Figure 5K) and *in vitro* (Figure 5L).

Having pinpointed the critical role for the two D-boxes in mediating APC^{Cdc20}-dependent destruction of Bim, we next examined whether ΔD1D2-Bim might be more potent in triggering apoptosis *in vivo*. Notably, by escaping Cdc20-mediated destruction, ΔD1D2-Bim expressing cells exhibited elevated expression of Bim (Figures 5M and S5D), and correspondingly displayed higher levels of basal Caspase 3 cleavage, compared with control and WT-Bim expressing cells (Figure 5M). More importantly, depletion of Cdc20 could efficiently trigger apoptosis in WT-Bim expressing cells by inducing Bim abundance (Figure 5M). On the other hand, depleting Cdc20 could not lead to further elevation of Bim abundance in ΔD1D2-expressing cells, thereby delivering minimal effects to Caspase 3 cleavage (Figure 5M), supporting that Cdc20 controls Bim stability largely through the two conserved D-boxes. Consistently, ΔD1D2-Bim expressing cells demonstrated a slower proliferation and an elevated sensitivity to Taxol compared with either control or WT-Bim expressing cells (Figures 5N and 5O). Hence, these results revealed that APC^{Cdc20} promotes the ubiquitination and subsequent destruction of the pro-apoptotic protein, Bim, largely in a D-box-dependent manner (Figure 5P).

Hyperactive Cdc20 contributes to chemo-resistance through targeting Bim for destruction in HTLV-I positive ATL cells

Given the critical role of Cdc20 in mitotic regulation, especially in the maintenance of SAC, recent studies began to reveal an oncogenic role for Cdc20 (Manchado et al., 2010). In keeping with this notion, Cdc20 was found to be frequently overexpressed in various human cancers including colorectal, breast, lung and bladder cancers (Kidokoro et al., 2008). Furthermore, in adult T cell leukemia (ATL) s, expression of the Human T-cell leukemia virus type 1 (HTLV-I) (Matsuoka and Jeang, 2007) encoding viral oncoprotein Tax resulted in a significant elevation of APC^{Cdc20} E3 ligase activity (Liu et al., 2005), but its importance in tumorigenesis remains unclear. Consistent with a previous study (Liu et al., 2005), we observed an inverse correlation between Tax expression and the abundance of various Cdc20 substrates including Cyclin B and Bim (Figure 6A). Furthermore, depletion of Cdc20

in Tax-positive SLB-1 and C91PL cells resulted in a significant upregulation of Bim (Figure 6B), supporting Cdc20 as a critical route through which Tax negatively regulates Bim abundance to promote ATL development. However, some of the Tax-positive ATL cell lines exhibited very low levels of Bim mRNA (Figure S6A), arguing that besides APC^{Cdc20}-mediated Bim ubiquitination, other unknown transcriptional mechanism(s) might also participate in regulating Bim expression.

More importantly, consistent with the observed inverse correlation between the protein levels of Tax and Bim, Tax-negative T cell lines including Jurkat, HuT78 and Molt4 were highly sensitive to Taxol (Figure 6C), with elevated apoptotic responses (Figures 6D, 6E and S6B). On the other hand, Tax-positive cells with lower Bim expression (Figure 6A), were more resistant to Taxol (Figure 6C). These distinct apoptotic responses between Tax-positive and Tax-negative T cells were similarly observed with other anti-cancer agents including Nocodazole (Figure S6C) and Fluorouracil (5-FU) (Figure S6D). Notably, depletion of Bim in Tax-negative HuT78 and Molt4 cells (Figure S6E) desensitized their apoptotic responses to Taxol (Figure 6F) and Nocodazole (Figure S6F). Consistently, decreasing Bim expression by Tax overexpression (Figures 6G and S6G), desensitized cellular response to Taxol (Figure 6H). Furthermore, in Tax expressing cells, there was a remarkable elevation of apoptosis in Cdc20-depleted cells in response to Taxol (Figures 6I–K, S6H–I), indicating that Tax might mainly function through activating APC^{Cdc20} to destabilize Bim and subsequently suppress apoptosis. In line with this finding, ectopic expression of Cdc20 in Tax-negative Jurkat and Molt4 cells, phenocopying both Tax-positive cells (Figure 6C) and ectopic overexpression of Tax (Figure 6H), led to a significant reduction in apoptosis by Taxol (Figures 6L–N, S6J–M).

We next examined whether loss of Cdc20 sensitizes Taxol-resistant Tax positive cells (Figure 6C) to Taxol treatment. Notably, depletion of Cdc20 in Tax positive C91PL cells resulted in an increase in Bim levels (Figure 6B) and consequently, increased apoptotic response to Taxol (Figure S6N). Furthermore, compared with control cells, Cdc20-depleted cells were more sensitive to Taxol-induced apoptosis, a phenotype that could be largely rescued by additional depletion of Bim (Figures 6O–Q, S6O–R). These results collectively support the notion that expression of Tax may allow the resulting ATL cells to evade cellular apoptosis mainly via an elevated destruction of Bim by APC^{Cdc20}.

Interestingly, although Tax-positive T cells acquired resistance to multiple chemotherapeutic drugs, compared to Tax-negative T cells, they are much more sensitive to the BH3-mimetic, ABT-737 (Cragg et al., 2009) that can induce apoptosis through inactivating the anti-apoptotic Bcl-2 family proteins, but not Mcl-1 (Figure S6S). Notably, when Tax-positive T cells were treated by Taxol together with ABT-737, ABT-737 sensitized their apoptotic responses to Taxol (Figures S6T–V). We reasoned that this might be in part due to the relatively higher expression of Bcl-2 in Tax-positive T cells with unclear mechanism(s) (Figure 6A). These cells are therefore more sensitive to the pan-Bcl-2 inhibitor, ABT-737, as depletion of Bcl-2 in Tax positive, but not Tax negative, cells significantly desensitized them to ABT-737 treatment (Figure S6W) (Deng et al., 2007).

Cdc20 knockdown induces chemo-radiation sensitization in head and neck cancer cells

As overexpression of Cdc20 has been observed in a wide spectrum of human cancers, next we intended to determine whether the biological significance for APC^{Cdc20}-mediated Bim ubiquitination also accounts for the tumorigenesis observed in other types of human cancers in the absence of Tax. Acquiring resistance to radiotherapy has been frequently observed in the clinic and often led to unfavorable therapeutic outcomes but the underlying molecular mechanisms remain largely elusive (Begg et al., 2011). Therefore, we designed an siRNA screening strategy to discover critical genes whose silencing sensitizes UMSCC-12 head and neck squamous carcinoma cells to γ-irradiation (Figure S7A).

Strikingly, among 23 confirmed radio-sensitizing hits out of a collection of 8,800 targeted genes in this siRNA library, six are components of the APC^{Cdc20} E3 ubiquitin ligase, including Cdc20, Cdc27, APC4, APC6, APC8 and Cdc26 (Figures 7A and S7B). Follow-up clonogenic assays confirmed that siRNA knockdown of Cdc20 and Cdc27 indeed sensitized UMSCC-12 cells to radiation (Figures S7C and S7D). We next determined the potential involvement of Bim, known to trigger apoptosis following DNA damage (Happo et al., 2010), in this process. We found that in UMSCC-12 cells, knockdown of endogenous Cdc20 (Figure 7B) or other APC core components including Cdc27 (Figure 7C), APC4 (Figure 7D), APC6 (Figure 7E) and APC8 (Figure 7F) caused a dramatic elevation of Bim, but not other BH3-only proteins such as Puma or Bid. More significantly, radio-sensitization by Cdc20-knockdown in UMSCC-12 cells was significantly abrogated by additional depletion of endogenous Bim (Figures 7G and S7E). Consistent with results obtained from human fibroblasts (Figure 2G), Cdc20 depletion-induced Bim stabilization could be reversed by re-introducing WT, but not inactive N-terminal Cdc20, in UMSCC-12 cells (Figure 7H). Thus, these results support the notion that depletion of Cdc20 caused an accumulation of its ubiquitin substrate, Bim, leading to radio-sensitization.

We also observed that Cdc20 knockdown in UMSCC-12 cells increased apoptosis induced by various chemo-drugs including Taxol, 5-FU and Etoposide (Figures 7I–J and S7G). Moreover, reintroduction of Cdc20 into Cdc20-depleted UMSCC-12 cells desensitized their apoptotic response to Taxol treatment (Figures 7K). It is noteworthy that unlike the observed Bim accumulation after depleting Cdh1 in HeLa and HCT116 cells (Figures 2A and 2B), Cdh1 knockdown in UMSCC-12 cells failed to induce Bim accumulation (Figure S7F). Consistently, depletion of Cdh1 failed to sensitize UMSCC-12 cells to radiation (Figure S7B). Thus, unlike Cdc20, Cdh1-mediated negative regulation of Bim may be more restricted to certain cellular contexts.

Taken together, these results, on one hand, emphasize a pivotal role of APC^{Cdc20} in governing apoptosis in UMSCC-12 cells, and on the other hand, suggest that destruction of Bim might be regulated by different upstream E3 ligases in different cellular contexts (Figure S3C). Importantly, compared with control cells, Bim-depleted UMSCC-12 cells were much more resistant to the DNA-damaging agent 5-FU (Figure S7H), advocating a critical role for Bim in DNA damage-induced apoptosis. Consistently, depletion of Bim in shCdc20-UMSCC-12 cells (Figures S7I) desensitized their apoptotic responses triggered by Cdc20 deletion, and partly restored their resistance to γ-irradiation (Figure 7G), Taxol, 5-FU and Etoposide (Figures 7J and S7J–K), arguing that the Cdc20/Bim axis is critical for

apoptosis induced by γ-irradiation and various anti-cancer chemotherapeutic agents under these experimental settings.

In keeping with an identified oncogenic role for Cdc20 (Manchado et al., 2010), we demonstrated that depleting endogenous Cdc20 in UMSCC-12 cells severely reduced their ability to form colonies *in vitro* upon treatment with various anti-cancer agents, including Taxol, 5-FU and Etoposide (Figures 7L–M and S7L). Ectopic expression of WT, but not the inactive N-terminal Cdc20, in shCdc20-UMSCC-12 cells largely desensitized their response to anti-cancer drug treatment (Figures 7N–O and S7M). Notably, Cdc20-depleted UMSCC-12 cells failed to form xenografts in nude mice (Figure S7N), supporting a crucial role for Cdc20 in controlling tumorigenesis. More importantly, simultaneous Bim knockdown in shCdc20-UMSCC-12 cells partly restored their chemo-resistance to various anti-cancer agents (Figures 7L–M and S7L), suggesting that Cdc20 might exert its oncogenic role in part by promoting the destruction of Bim to bypass apoptosis triggered by anti-cancer treatments such as chemotherapeutic agents or γ-irradiation.

Given the critical role for Puma and Bid in Bak/Bax-mediated mitochondrial apoptotic pathway (Ren et al., 2010), we examined whether besides Bim, Puma and Bid are also important for Cdc20 depletion induced apoptosis. Notably, neither Puma nor Bid protein levels fluctuated across the cell cycle (Figures 1A and 1C), and their abundance remained unchanged after Cdc20 depletion (Figures 2A–C, 2H and 7B), suggesting that they are unlikely to be APC^{Cdc20} substrates. In contrast to Bim, neither Puma nor Bid levels were induced by MG132 (Figure 2J), and ectopic Cdc20 expression failed to induce Puma or Bid degradation (Figure S5J). Notably, depletion of Bim and Puma, but not Bid, could largely suppress Cdc20 deletion-triggered apoptosis (Figures 7P and S7O). Similarly, the inhibition of apoptosis (Figures 7Q and S7P) and the restoration of clonogenic potential (Figures 7R–S and S7Q) were observed after depleting Bim or Puma, but not Bid, in shCdc20-UMSCC-12 cells. Since our biochemical assays excluded Puma as a *bona fide* Cdc20 substrate, we reasoned that Puma knockdown might indirectly affect Cdc20 depletion-induced apoptosis. In keeping with this notion, depletion of Puma could enhance endogenous interaction between Bim and Bcl-2 (Figure S7R). Recent studies from multiple groups suggested that the balance between a cohort of pro-apoptotic proteins such as Puma, Bim, Bid and a cohort of anti-apoptotic proteins including Bcl-2, Bcl-xL and Mcl-1 determines the cellular apoptotic status (Certo et al., 2006; Chipuk et al., 2010; Gavathiotis et al., 2008). Furthermore, depletion of Cdc20 stabilized Bim to trigger apoptosis by either binding Bcl-2 to free Bax/Bak or by directly binding Bax/Bak (Kuwana et al., 2005; Letai et al., 2002). Therefore, in Cdc20-depleted cells, depletion of otherwise elevated Bim could block cellular apoptosis. On the other hand, as both Bim and Puma can bind to Bcl-2 family proteins and Bax/Bak (Chipuk et al., 2010), depletion of Puma might lead to the release of free Bcl-2 or Bax/Bak, therefore shifting the interactome among pro-apoptotic and anti-apoptotic proteins (Deng et al., 2007) to phenocopy Bim depletion (Figure S7R).

DISCUSSION

Our studies reveal a crucial role for the Cdc20-Bim signaling axis in promoting the survival of cancer cells, indicating that aberrant activation of Cdc20 in various human cancers could

allow the acquisition of chemo- or radio-resistance in part by promoting Bim destruction to evade apoptosis triggered by γ-irradiation and/or chemotherapeutic agents. As many components of the apoptosis signaling pathway have long been utilized as efficient anti-cancer targets (Rufini and Melino, 2011), our work strongly argues for Cdc20 as an attractive therapeutic drug target. To this end, inactivating the APC by an IR-mimetic inhibitor, pro-TAME, which targets both APC^{Cdc20} and APC^{Cdh1}, also induced cell death in multiple cancer cell lines (Zeng et al., 2010). We also found that due to activation of ERK signaling, prolonged Taxol treatment unexpectedly led to decreased expression of Bim, thereby compromising the anti-tumor effects of Taxol (Figure S1D). Hence, we propose that a rationally designed specific Cdc20 inhibitor rather than a pan-APC inhibitor might more efficiently trigger tumor cell apoptosis by elevating the abundance of the pro-apoptotic protein, Bim (Figure 7T). Moreover, our results also indicate that the observed synergistic anti-cancer effects of Taxol and MAPK inhibitors (McDaid et al., 2005) might function in part by blocking ERK-mediated destruction of Bim to trigger apoptosis.

Interestingly, Cdc20 activity was reported to be inhibited by DNA damage-induced PKA phosphorylation (Searle et al., 2004). Meantime, PKA-mediated phosphorylation of Bim at Ser83 was reported to stabilize Bim (Moujalled et al., 2011). As Ser83 is located within the second D-box motif of Bim (Figure S5E), this prompted us to examine whether the phosphorylation at Ser83 would affect the interaction between Bim and Cdc20. Strikingly, behaving similarly to the D-box-deleted mutant ΔD1D2, the phospho-mimetic mutant S83D is deficient in binding Cdc20 (Figures S5A–C). Consistently, we observed a dramatic decrease of binding between Cdc20 and Bim after being treated with DNA damage agents (Figure S5F). These results indicate that PKA-mediated phosphorylation of Bim (Figure S5E) could disrupt Cdc20-mediated destruction of Bim to trigger apoptosis (Figure S5G). Similar phosphorylation-mediated impairment of substrate recognition has been reported for Skp2 (Figure S5H) and Cdc6 (Figure S5I) to evade APC^{Cdh1}-mediated proteolysis (Gao et al., 2009; Mailand and Diffley, 2005).

Given the pivotal role of the pro-apoptotic protein Bim in governing apoptosis, several E3 ligases have been reported to negatively regulate Bim stability including c-Cbl and ElonginB/C-Cullin2-CIS (Thien et al., 2010; Zhang et al., 2008). Recently, it has been reported that Bim is ubiquitinated by SCFβ-TRCP (Dehan et al., 2009) in an ERK/RSK phosphorylation dependent manner, and occurs mainly in the late G1 and S phases (Dehan et al., 2009). However, our results here suggested that APC^{Cdc20} is a physiological E3 ligase that promotes the ubiquitination and destruction of the tumor suppressor, Bim, thus conferring the resistance of cancer cells to chemo-radiation. Therefore, our findings collectively shed light into the oncogenic role of Cdc20 and further provide a rationale for developing specific Cdc20 inhibitors as efficient anti-cancer agents (Figure 7T).

EXPERIMENTAL PROCEDURES

siRNA Library Screening

The Dharmacon siRNA libraries of ~8,800 druggable genes, consisting of 1) ~7,422 druggable genes (Human ON-TARGET*plus* SMARTpool Druggable Genome); 2) 788 kinase genes (Human ON-TARGETplus SMARTpool siRNA Library - Protein Kinases);

and 3) 580 GPCR genes (SMARTpool-G Protein-Coupled Receptors) were screened using a 5-day ATP-lite assay, mimicking colony-formation. Detailed methods can be found in the Supplemental Information online.

γ-irradiation Clonogenic Assays

Clonogenic assays were performed as described previously (Zheng et al., 2008). Briefly, UMSCC-12 cells after lentivirus-based shRNA silencing or siRNA oligonucleotide transfection were seeded in 60-mm dish in triplicates. The next day, cells were exposed to different doses of γ-irradiation followed by incubation at 37°C for 7 to 9 days. The colonies formed were fixed and the surviving fraction was determined by the proportion of seeded cells following irradiation to form colonies relative to untreated cells. SER (Sensitization Enhancement Ratio) was calculated as the ratio of the mean inactivation dose under control siRNA conditions divided by the mean inactivation dose after Cdc20 silencing.

FACS Analysis

Cells synchronized with serum starvation and reefed or Nocodazole-arrest and release were collected at the indicated time points and stained with propidium iodide (Roche) according to the manufacturer's instructions. Stained cells were sorted with a Dako-Cytomation MoFlo sorter (Dako) at the Dana-Farber Cancer Institute FACS core facility.

Annexin-V/7-AAD Double Staining

For detection of apoptosis, cells treated with various drugs were co-stained with Annexin-V–PE and 7-AAD (Annexin V-PE Apoptosis Detection Kit I, BD Bioscience) according to the manufacturer's instructions. Stained cells were sorted with a Dako-Cytomation MoFlo sorter (Dako) at the Dana-Farber Cancer Institute FACS core facility.

Clonogenic Survival and Soft Agar Assays

For clonogenic survival assays, 1,000 cells were plated into 6-well plate and treated with the indicated anti-cancer agents where indicated. After 14 days, cells were stained using crystal violet and colonies larger than 50 cells were stained and quantified.

For soft agar assays, cells (3,000 per well) were seeded in 0.5% low-melting-point agarose in DMEM with 10% FBS, layered onto 0.8% agarose in DMEM/10% FBS. The plates were kept in the cell culture incubator for 30 days after which the colonies >50 μm were counted under a light microscope, and the colony numbers were counted and quantified.

siRNA

siRNA oligos were transfected into subconfluent cells with Oligofectamine or Lipofectamine 2000 (Invitrogen) according to the manufacturer's instructions. Human siRNA oligos against Cdh1 and Cdc20 have been described before (Wan et al., 2011). Human siRNA oligo that can deplete both β-TRCP1 and β-TRCP2 (sense, 5'-AAGUGGAAUUUGUGGAACAUC-3') has been validated previously (Jin et al., 2003). E2F-1 scramble siRNA oligo was purchased from Dharmacon and served as a negative control.

In Vitro Binding Assays

Binding to immobilized GST proteins was performed as described previously (Wan et al., 2011).

Statistical Analysis

All quantitative data were presented as the mean ± SEM or the mean ± SD as indicated of at least three independent experiments by Student's *t* test for between group differences. The $p < 0.05$ was considered as statistically significant.

Additional experimental procedures/reagent information, including Cell Culture and Synchronization, Degradation and Ubiquitination Analysis, and Tumorigenesis Assay is in the Supplemental Information online.

Supplementary Material

Refer to Web version on PubMed Central for supplementary material.

Acknowledgments

We thank members of Wei laboratory for critical reading of the manuscript, Roya Khosravi-Far, Gutian Xiao, Christophe P. Nicot, Peter Jackson, Matthew Meyerson, William Hahn, Frederic D. Sigoillot and Randall W. King for providing reagents, Timothy J. Mitchison, Randall W. King and Susan E. Morgan-Lappe for helpful suggestions. W.W. is a Leukemia and Lymphoma Society Scholar and ACS Research Scholar. This work was supported in part by the NIH grants (W.W., GM089763 and GM094777; Y.S., CA118762 and CA156744; and M.W.K., GM39023). L.W. was supported by Lady Tata Memorial Trust International Award for Research in Leukemia. This work was also partially supported by a research grant from University of Michigan Comprehensive Cancer Center to Y.S.

REFERENCES

Amador V, Ge S, Santamaria PG, Guardavaccaro D, Pagano M. APC/C(Cdc20) controls the ubiquitin-mediated degradation of p21 in prometaphase. Mol Cell. 2007; 27:462–473. [PubMed: 17679094]

Begg AC, Stewart FA, Vens C. Strategies to improve radiotherapy with targeted drugs. Nat Rev Cancer. 2011; 11:239–253. [PubMed: 21430696]

Bouillet P, Metcalf D, Huang DC, Tarlinton DM, Kay TW, Kontgen F, Adams JM, Strasser A. Proapoptotic Bcl-2 relative Bim required for certain apoptotic responses, leukocyte homeostasis, and to preclude autoimmunity. Science. 1999; 286:1735–1738. [PubMed: 10576740]

Brooks CL, Gu W. p53 regulation by ubiquitin. FEBS Lett. 2011; 585:2803–2809. [PubMed: 21624367]

Certo M, Del Gaizo Moore V, Nishino M, Wei G, Korsmeyer S, Armstrong SA, Letai A. Mitochondria primed by death signals determine cellular addiction to antiapoptotic BCL-2 family members. Cancer Cell. 2006; 9:351–365. [PubMed: 16697956]

Chipuk JE, Moldoveanu T, Llambi F, Parsons MJ, Green DR. The BCL-2 family reunion. Mol Cell. 2010; 37:299–310. [PubMed: 20159550]

Cragg MS, Harris C, Strasser A, Scott CL. Unleashing the power of inhibitors of oncogenic kinases through BH3 mimetics. Nat Rev Cancer. 2009; 9:321–326. [PubMed: 19343035]

Dehan E, Bassermann F, Guardavaccaro D, Vasiliver-Shamis G, Cohen M, Lowes KN, Dustin M, Huang DC, Taunton J, Pagano M. betaTrCP- and Rsk1/2-mediated degradation of BimEL inhibits apoptosis. Mol Cell. 2009; 33:109–116. [PubMed: 19150432]

Deng J, Carlson N, Takeyama K, Dal Cin P, Shipp M, Letai A. BH3 profiling identifies three distinct classes of apoptotic blocks to predict response to ABT-737 and conventional chemotherapeutic agents. Cancer Cell. 2007; 12:171–185. [PubMed: 17692808]

Fang G, Yu H, Kirschner MW. The checkpoint protein MAD2 and the mitotic regulator CDC20 form a ternary complex with the anaphase-promoting complex to control anaphase initiation. Genes Dev. 1998; 12:1871–1883. [PubMed: 9637688]

Gao D, Inuzuka H, Tseng A, Chin RY, Toker A, Wei W. Phosphorylation by Akt1 promotes cytoplasmic localization of Skp2 and impairs APCCdh1-mediated Skp2 destruction. Nat Cell Biol. 2009; 11:397–408. [PubMed: 19270695]

Gascoigne KE, Taylor SS. Cancer cells display profound intra- and interline variation following prolonged exposure to antimitotic drugs. Cancer Cell. 2008; 14:111–122. [PubMed: 18656424]

Gavathiotis E, Suzuki M, Davis ML, Pitter K, Bird GH, Katz SG, Tu HC, Kim H, Cheng EH, Tjandra N, et al. BAX activation is initiated at a novel interaction site. Nature. 2008; 455:1076–1081. [PubMed: 18948948]

Gross A, McDonnell JM, Korsmeyer SJ. BCL-2 family members and the mitochondria in apoptosis. Genes Dev. 1999; 13:1899–1911. [PubMed: 10444588]

Hagting A, Den Elzen N, Vodermaier HC, Waizenegger IC, Peters JM, Pines J. Human securin proteolysis is controlled by the spindle checkpoint and reveals when the APC/C switches from activation by Cdc20 to Cdh1. J Cell Biol. 2002; 157:1125–1137. [PubMed: 12070128]

Happo L, Cragg MS, Phipson B, Haga JM, Jansen ES, Herold MJ, Dewson G, Michalak EM, Vandenberg CJ, Smyth GK, et al. Maximal killing of lymphoma cells by DNA damage-inducing therapy requires not only the p53 targets Puma and Noxa, but also Bim. Blood. 2010; 116:5256–5267. [PubMed: 20829369]

Hara H, Friedlander RM, Gagliardini V, Ayata C, Fink K, Huang Z, Shimizu-Sasamata M, Yuan J, Moskowitz MA. Inhibition of interleukin 1beta converting enzyme family proteases reduces ischemic and excitotoxic neuronal damage. Proc Natl Acad Sci U S A. 1997; 94:2007–2012. [PubMed: 9050895]

Harper JW, Burton JL, Solomon MJ. The anaphase-promoting complex: it's not just for mitosis any more. Genes Dev. 2002; 16:2179–2206. [PubMed: 12208841]

Huang HC, Shi J, Orth JD, Mitchison TJ. Evidence that mitotic exit is a better cancer therapeutic target than spindle assembly. Cancer Cell. 2009; 16:347–358. [PubMed: 19800579]

Inuzuka H, Shaik S, Onoyama I, Gao D, Tseng A, Maser RS, Zhai B, Wan L, Gutierrez A, Lau AW, et al. SCF(FBW7) regulates cellular apoptosis by targeting MCL1 for ubiquitylation and destruction. Nature. 2011; 471:104–109. [PubMed: 21368833]

Jiang J, Jedinak A, Sliva D. Ganodermanontriol (GDNT) exerts its effect on growth and invasiveness of breast cancer cells through the down-regulation of CDC20 and uPA. Biochem Biophys Res Commun. 2011; 415:325–329. [PubMed: 22033405]

Jin J, Shirogane T, Xu L, Nalepa G, Qin J, Elledge SJ, Harper JW. SCFbeta-TRCP links Chk1 signaling to degradation of the Cdc25A protein phosphatase. Genes Dev. 2003; 17:3062–3074. [PubMed: 14681206]

Kato T, Daigo Y, Aragaki M, Ishikawa K, Sato M, Kaji M. Overexpression of CDC20 predicts poor prognosis in primary non-small cell lung cancer patients. J Surg Oncol. 2012; 106:423–430. [PubMed: 22488197]

Kidokoro T, Tanikawa C, Furukawa Y, Katagiri T, Nakamura Y, Matsuda K. CDC20, a potential cancer therapeutic target, is negatively regulated by p53. Oncogene. 2008; 27:1562–1571. [PubMed: 17873905]

King RW, Deshaies RJ, Peters JM, Kirschner MW. How proteolysis drives the cell cycle. Science. 1996; 274:1652–1659. [PubMed: 8939846]

Kuwana T, Bouchier-Hayes L, Chipuk JE, Bonzon C, Sullivan BA, Green DR, Newmeyer DD. BH3 domains of BH3-only proteins differentially regulate Bax-mediated mitochondrial membrane permeabilization both directly and indirectly. Mol Cell. 2005; 17:525–535. [PubMed: 15721256]

Letai A, Bassik MC, Walensky LD, Sorcinelli MD, Weiler S, Korsmeyer SJ. Distinct BH3 domains either sensitize or activate mitochondrial apoptosis, serving as prototype cancer therapeutics. Cancer Cell. 2002; 2:183–192. [PubMed: 12242151]

Liu B, Hong S, Tang Z, Yu H, Giam CZ. HTLV-I Tax directly binds the Cdc20-associated anaphase-promoting complex and activates it ahead of schedule. Proc Natl Acad Sci U S A. 2005; 102:63–68. [PubMed: 15623561]

Mailand N, Diffley JF. CDKs promote DNA replication origin licensing in human cells by protecting Cdc6 from APC/C-dependent proteolysis. Cell. 2005; 122:915–926. [PubMed: 16153703]

Manchado E, Guillamot M, de Carcer G, Eguren M, Trickey M, Garcia-Higuera I, Moreno S, Yamano H, Canamero M, Malumbres M. Targeting Mitotic Exit Leads to Tumor Regression In Vivo: Modulation by Cdk1, Mastl, and the PP2A/B55alpha, delta Phosphatase. Cancer Cell. 2010; 18:641–654. [PubMed: 21156286]

Matsuoka M, Jeang KT. Human T-cell leukaemia virus type 1 (HTLV-1) infectivity and cellular transformation. Nat Rev Cancer. 2007; 7:270–280. [PubMed: 17384582]

McDaid HM, Lopez-Barcons L, Grossman A, Lia M, Keller S, Perez-Soler R, Horwitz SB. Enhancement of the therapeutic efficacy of taxol by the mitogen-activated protein kinase kinase inhibitor CI-1040 in nude mice bearing human heterotransplants. Cancer Res. 2005; 65:2854–2860. [PubMed: 15805287]

Moujalled D, Weston R, Anderton H, Ninnis R, Goel P, Coley A, Huang DC, Wu L, Strasser A, Puthalakath H. Cyclic-AMP-dependent protein kinase A regulates apoptosis by stabilizing the BH3-only protein Bim. EMBO Rep. 2011; 12:77–83. [PubMed: 21151042]

Nilsson J, Yekezare M, Minshull J, Pines J. The APC/C maintains the spindle assembly checkpoint by targeting Cdc20 for destruction. Nat Cell Biol. 2008; 10:1411–1420. [PubMed: 18997788]

Reddy SK, Rape M, Margansky WA, Kirschner MW. Ubiquitination by the anaphase-promoting complex drives spindle checkpoint inactivation. Nature. 2007; 446:921–925. [PubMed: 17443186]

Reimann JD, Gardner BE, Margottin-Goguet F, Jackson PK. Emi1 regulates the anaphase-promoting complex by a different mechanism than Mad2 proteins. Genes Dev. 2001; 15:3278–3285. [PubMed: 11751633]

Ren D, Tu HC, Kim H, Wang GX, Bean GR, Takeuchi O, Jeffers JR, Zambetti GP, Hsieh JJ, Cheng EH. BID, BIM, and PUMA are essential for activation of the BAX- and BAK-dependent cell death program. Science. 2010; 330:1390–1393. [PubMed: 21127253]

Rufini A, Melino G. Cell death pathology: the war against cancer. Biochem Biophys Res Commun. 2011; 414:445–450. [PubMed: 21971555]

Searle JS, Schollaert KL, Wilkins BJ, Sanchez Y. The DNA damage checkpoint and PKA pathways converge on APC substrates and Cdc20 to regulate mitotic progression. Nat Cell Biol. 2004; 6:138–145. [PubMed: 14743219]

Tan TT, Degenhardt K, Nelson DA, Beaudoin B, Nieves-Neira W, Bouillet P, Villunger A, Adams JM, White E. Key roles of BIM-driven apoptosis in epithelial tumors and rational chemotherapy. Cancer Cell. 2005; 7:227–238. [PubMed: 15766661]

Thien CB, Dagger SA, Steer JH, Koentgen F, Jansen ES, Scott CL, Langdon WY. c-Cbl promotes T cell receptor-induced thymocyte apoptosis by activating the phosphatidylinositol 3-kinase/Akt pathway. J Biol Chem. 2010; 285:10969–10981. [PubMed: 20133944]

Wan L, Zou W, Gao D, Inuzuka H, Fukushima H, Berg AH, Drapp R, Shaik S, Hu D, Lester C, et al. Cdh1 regulates osteoblast function through an APC/C-independent modulation of Smurf1. Mol Cell. 2011; 44:721–733. [PubMed: 22152476]

Wei W, Kaelin WG Jr. Good COP1 or bad COP1? In vivo veritas. J Clin Invest. 2011; 121:1263–1265. [PubMed: 21403396]

Wertz IE, Kusam S, Lam C, Okamoto T, Sandoval W, Anderson DJ, Helgason E, Ernst JA, Eby M, Liu J, et al. Sensitivity to antitubulin chemotherapeutics is regulated by MCL1 and FBW7. Nature. 2011; 471:110–114. [PubMed: 21368834]

Wu T, Merbl Y, Huo Y, Gallop JL, Tzur A, Kirschner MW. UBE2S drives elongation of K11-linked ubiquitin chains by the anaphase-promoting complex. Proc Natl Acad Sci U S A. 2010; 107:1355–1360. [PubMed: 20080579]

Youle RJ, Strasser A. The BCL-2 protein family: opposing activities that mediate cell death. Nat Rev Mol Cell Biol. 2008; 9:47–59. [PubMed: 18097445]

Yu H. Cdc20: a WD40 activator for a cell cycle degradation machine. Mol Cell. 2007; 27:3–16. [PubMed: 17612486]

Zeng X, Sigoillot F, Gaur S, Choi S, Pfaff KL, Oh DC, Hathaway N, Dimova N, Cuny GD, King RW. Pharmacologic inhibition of the anaphase-promoting complex induces a spindle checkpoint-

dependent mitotic arrest in the absence of spindle damage. Cancer Cell. 2010; 18:382–395. [PubMed: 20951947]

Zhang W, Cheng GZ, Gong J, Hermanto U, Zong CS, Chan J, Cheng JQ, Wang LH. RACK1 and CIS mediate the degradation of BimEL in cancer cells. J Biol Chem. 2008; 283:16416–16426. [PubMed: 18420585]

Zheng M, Morgan-Lappe SE, Yang J, Bockbrader KM, Pamarthy D, Thomas D, Fesik SW, Sun Y. Growth inhibition and radiosensitization of glioblastoma and lung cancer cells by small interfering RNA silencing of tumor necrosis factor receptor-associated factor 2. Cancer Res. 2008; 68:7570–7578. [PubMed: 18794145]

HIGHLIGHTS

- Bim expression is repressed during M phase of cell cycle, when Cdc20 is most active
- Cdc20 promotes Bim ubiquitination and destruction in a D-box dependent manner
- Hyper-activation of Cdc20 by Taxol confers chemo-resistance via Bim destruction
- Cdc20 knockdown sensitizes cancer cells to chemo-radiation via Bim accumulation

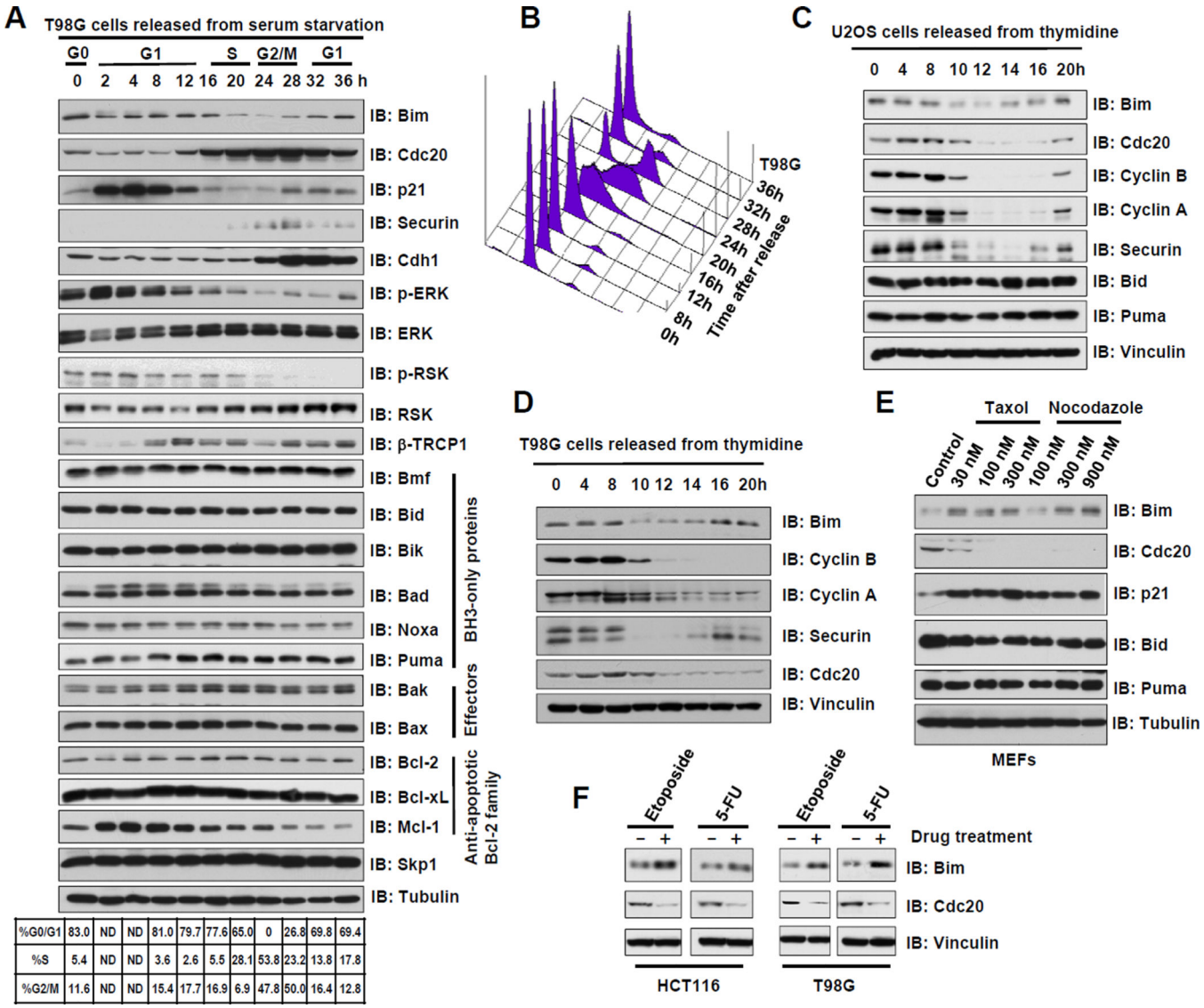

Figure 1. The destruction of the pro-apoptotic protein, Bim, is accelerated during the mitosis where APC^{Cdc20} is most active

(A) Immunoblot (IB) analysis of whole cell lysates (WCL) derived from T98G cells synchronized in G0 by serum starvation followed by serum re-addition for the indicated periods of time.

(B) FACS analysis was performed to monitor cell cycle changes for T98G cells in **A**.

(C–D) IB analysis of WCL derived from U2OS (**C**) and T98G (**D**) cells synchronized at the G1/S boundary by double-thymidine block then released back into the cell cycle for the indicated periods of time.

(E) IB analysis of WCL derived from MEFs treated with increasing doses of Taxol or Nocodazole for 48 hours before harvesting for IB analysis.

(F) IB analysis of WCL derived from HCT116 and T98G cells treated with 10 μM Etoposide or 10 μg/ml 5-FU for 48 hours before harvesting for IB analysis.

(See also Figure S1)

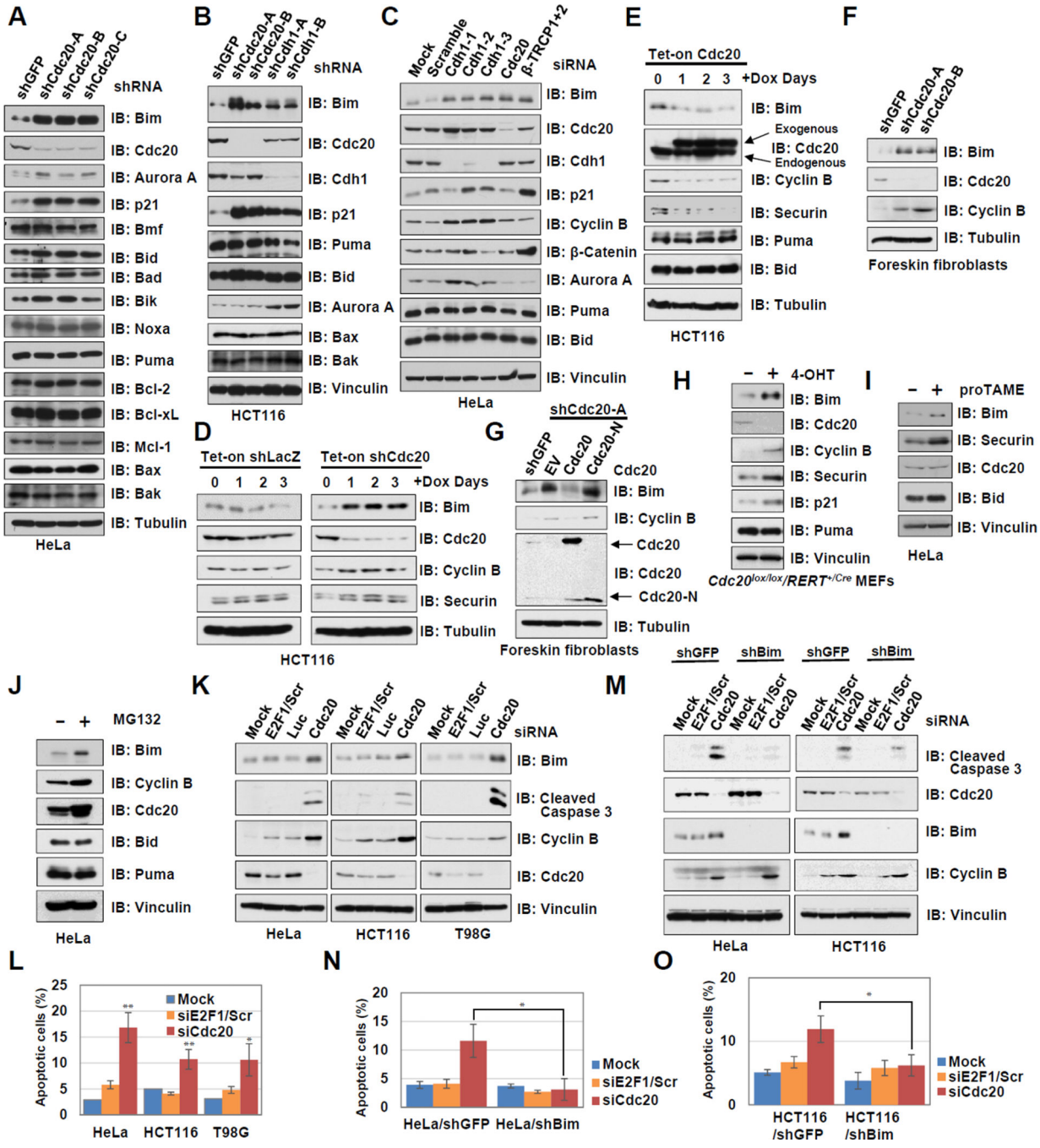

Figure 2. Cdc20 deficiency leads to Bim upregulation

(A–B) Immunoblot (IB) analysis of HeLa (**A**) or HCT116 (**B**) cells infected with the indicated lentiviral shRNA constructs. The infected cells were selected with 1 μg/ml puromycin for 72 hours to eliminate the non-infected cells before harvesting.

(C) IB analysis of whole cell lysates (WCL) derived from HeLa cells transfected with the indicated siRNA oligos. Mock transfection and E2F1 scramble siRNA (Scramble) were used as negative controls.

(D) HCT116 cells were infected with Tet-inducible shLacZ and shCdc20 lentiviral vectors and were selected with 1 μg/ml puromycin for 72 hours to eliminate non-infected cells. Afterwards, 100 ng/ml doxycycline was added to the generated cell lines for the indicated time periods before harvesting.

(E) HCT116 cells were infected with the indicated pTRIPZ lentiviral vectors and were selected with 1 μg/ml puromycin for 72 hours to eliminate non-infected cells. Afterwards, 100 ng/ml doxycycline was added for the indicated time periods before harvesting.

(F) IB analysis of hTERT immortalized human primary foreskin fibroblasts infected with the indicated lentiviral shRNA constructs. The infected cells were selected with 1 μg/ml puromycin for 72 hours to eliminate the non-infected cells before harvesting.

(G) IB analysis of hTERT immortalized human primary foreskin fibroblasts infected with the indicated lentiviral shRNA constructs together with the indicated retroviral pWZL-Cdc20-expression vector. As the shCdc20-A targets a specific sequence in the 3-UTR of Cdc20 mRNA, the ectopically expressed various Cdc20 cDNAs lacking 3-UTR are resistant to shCdc20-A. The infected cells were selected with 1 μg/ml puromycin and 5 μg/ml blasticidin for 72 hours to eliminate the non-infected cells before harvesting.

(H) IB analysis of WCL derived from $Cdc20^{lox/lox}/RERT^{+/Cre}$ MEFs untreated or treated with 0.5 μM 4-OHT for 24 hours to induce the depletion of endogenous Cdc20. 10 μM Z-VAD-fmk was added to inhibit caspase-dependent cell death.

(I) IB analysis of WCL derived from HeLa cells treated with 12 μM of the specific APC inhibitor pro-TAME or DMSO as a negative control for 24 hours.

(J) IB analysis of WCL derived from HeLa cells treated with DMSO or 10 μM of the 26S proteasome inhibitor MG132 for 12 hours.

(K) IB analysis of WCL derived from HCT116, HeLa or T98G cells transfected with the indicated siRNA oligos. Mock transfection, luciferase (Luc) and E2F1 scramble siRNA (E2F1/Scr) were used as negative controls.

(L) Quantification of Annexin V and 7-AAD double staining of the indicated cells described in (**K**) to examine the effects of Cdc20 depletion towards cellular apoptosis. Annexin V positive stained cells were considered apoptotic cells. Data are shown as mean±SD for three independent experiments (** $p < 0.001$, * $p < 0.05$).

(M) IB analysis of WCL derived from shGFP or shBim infected HCT116 and HeLa cells transfected with the indicated siRNA oligos. Mock transfection and E2F1 scramble siRNA (E2F1/Scr) were used as negative controls.

(N–O) Quantification of Annexin V and 7-AAD double staining of the indicated cells described in (**M**) to examine the effects of Cdc20 depletion towards cellular apoptosis. Annexin V positive stained cells were considered apoptotic cells. Data are shown as mean ±SD for three independent experiments (* $p < 0.05$).

(See also Figure S2)

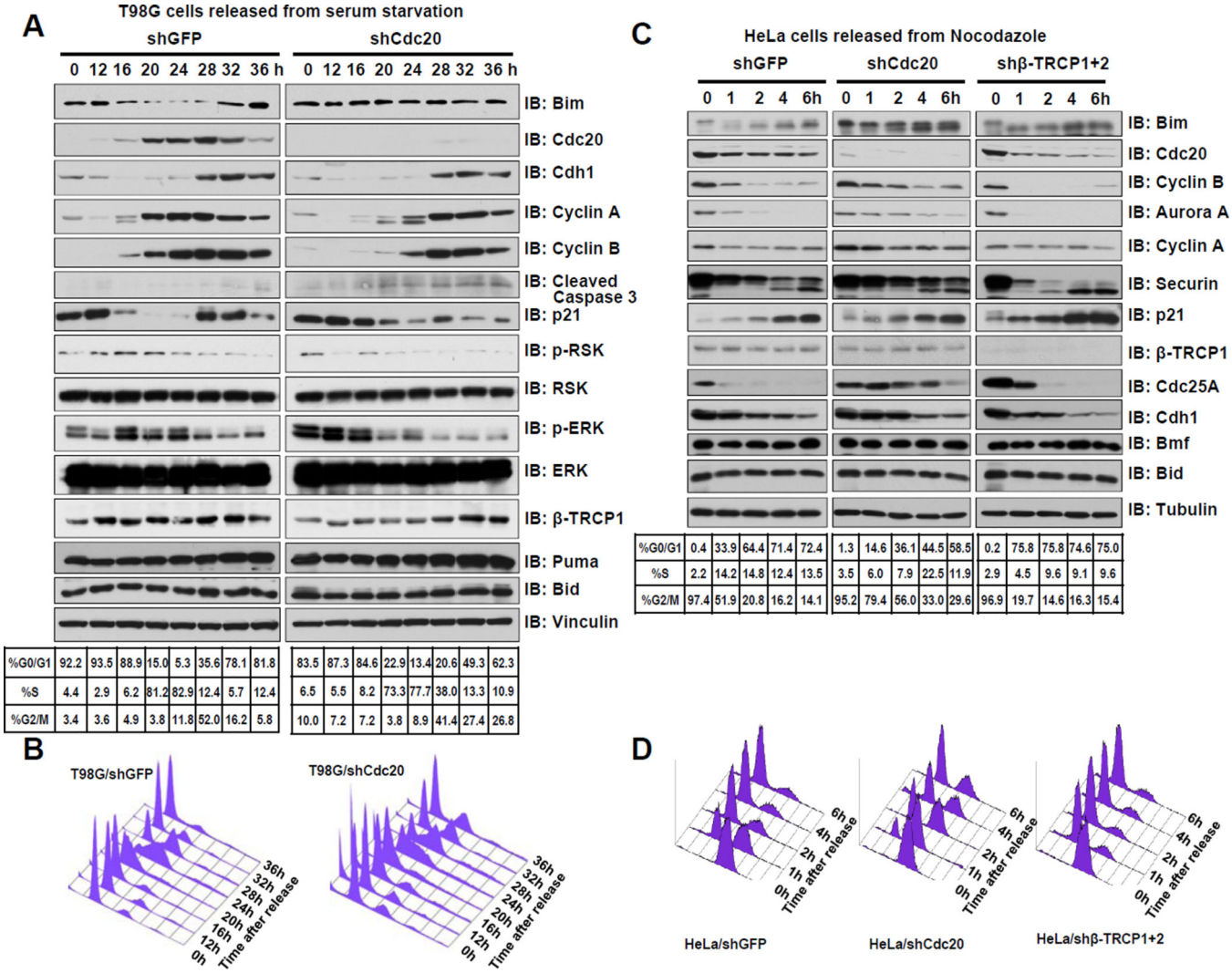

Figure 3. Bim is stabilized in Cdc20-depleted M phase cells

(A–B) T98G cells were infected with the indicated lentiviral shRNA constructs followed by selection with 1 μg/ml puromycin for 72 hours to eliminate the non-infected cells. The resulting cells were further synchronized in G0 by serum starvation followed by serum re-addition for the indicated periods of time (**A**). FACS analysis was performed to monitor the corresponding cell cycle changes (**B**).

(C–D) HeLa cells were infected with the indicated lentiviral shRNA constructs followed by selection with 1 μg/ml puromycin for 72 hours to eliminate the non-infected cells. The resulting cells were further synchronized in M phase by Nocodazole block then released back into the cell cycle for the indicated periods of time (**C**). FACS analysis was performed to monitor the corresponding cell cycle changes (**D**).

(See also Figure S3)

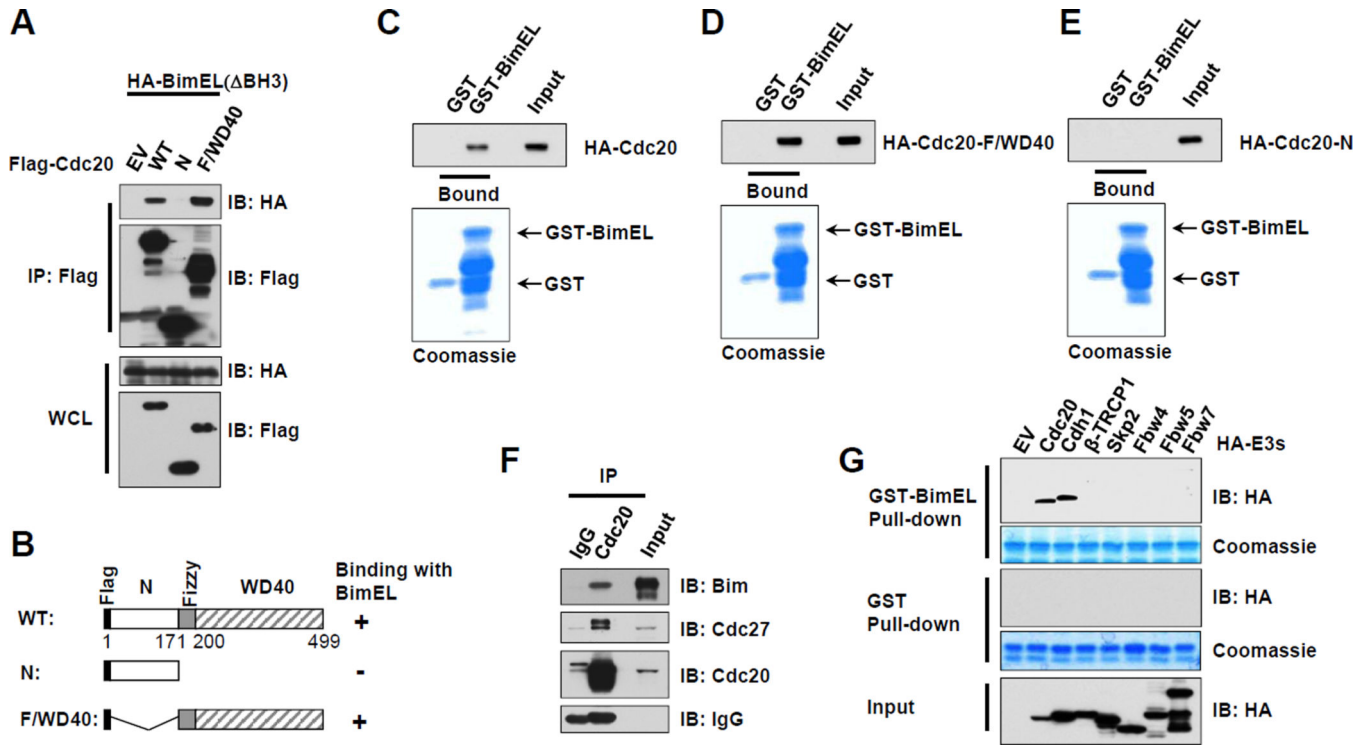

Figure 4. Bim specifically interacts with the C-terminal WD40 repeats motif of Cdc20

(A) Immunoblot (IB) analysis of whole cell lysates (WCL) and immunoprecipitates (IP) derived from 293T cells transfected with HA-ΔBH3-BimEL and the indicated Cdc20 constructs. Thirty hours post transfection, cells were pre-treated with 10 μM MG132 for 10 hours to block the proteasome pathway before harvesting.

(B) Schematic representation of the various Cdc20 truncation mutants used in this study.

(C–E) 293T cells were transfected with WT (**C**), WD40 (**D**) or N-terminal (**E**) HA-tagged Cdc20. 40 hours post-transfection, WCL were recovered to perform GST pull-down analysis with GST and GST-Bim proteins.

(F) IB analysis of WCL and anti-Cdc20 IP derived from HeLa cells. Mouse IgG was used as a negative control for the IP process, cells were pre-treated with 10 μM MG132 for 10 hours to block the proteasome pathway before harvesting.

(G) 293T cells were transfected with HA-tagged APC or SCF substrate receptor proteins and 40 hours post-transfection, whole cell lysates (WCL) were recovered to perform GST pull-down analysis with purified GST-Bim, or GST as a negative control.

(See also Figure S4)

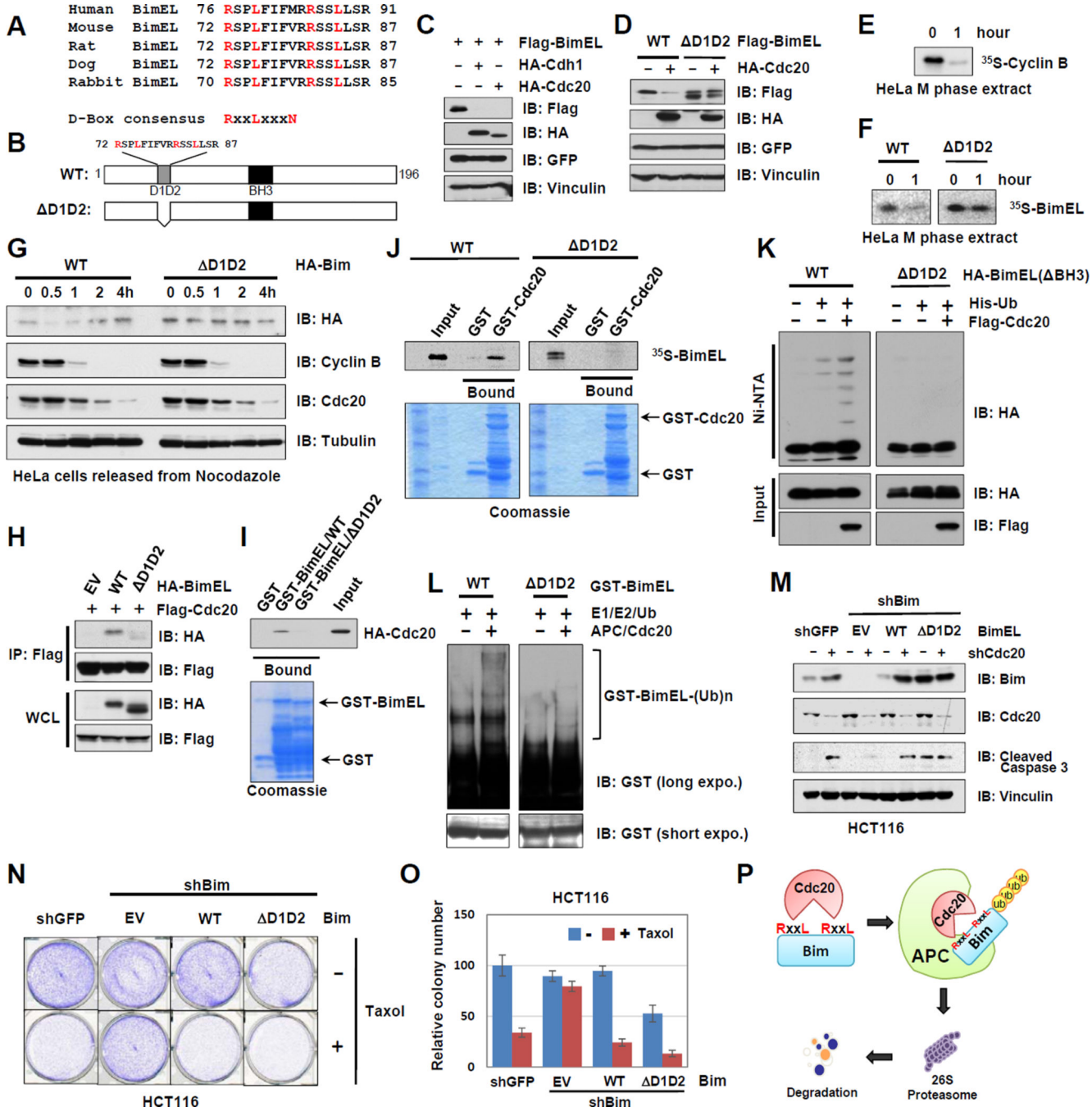

Figure 5. Cdc20 promotes the ubiquitination and degradation of Bim in a D-box-dependent manner

(A) Sequence alignment of the D-boxes containing region between BimEL proteins from various species.

(B) Schematic representation of the D-boxes deletion mutant used in the following studies.

(C) Immunoblot (IB) analysis of whole cell lysates (WCL) derived from HeLa cells transfected with HA-Cdh1 or HA-Cdc20 and Flag-BimEL constructs. 10 μM Z-VAD-fmk was added to inhibit caspase-dependent cell death.

(D) IB analysis of WCL derived from HeLa cells transfected with HA-Cdc20 and the indicated Flag-BimEL constructs. 10 μM Z-VAD-fmk was added to inhibit caspase-dependent cell death.

(E–F) Autoradiography of ^{35}S-labelled Cyclin B (**E**), which was used as a positive control of the APC^{Cdc20} substrate, as well as ^{35}S-labelled WT- and ΔD1D2-BimEL (**F**) after incubating with purified HeLa M-phase extract for 1 hour followed by SDS-PAGE.

(G) HeLa cells were transfected with the indicated HA-Bim constructs. 24 hours post-transfection, the resulting cells were synchronized in M phase by Nocodazole block then released back into the cell cycle for the indicated periods of time before harvesting for IB analysis.

(H) IB analysis of WCL and IP derived from 293T cells transfected with BH3-deleted versions of HA-WT-BimEL and HA-ΔD1D2-BimEL together with the Flag-Cdc20 construct. Thirty hours post-transfection, cells were pre-treated with 10 μM MG132 for 10 hours to block the proteasome pathway before harvesting.

(I) 293T cells were transfected with HA-Cdc20 and 40 hours post-transfection, whole cell lysates (WCL) were recovered to perform GST pull-down analysis with GST and the indicated GST-Bim proteins.

(J) Autoradiography of ^{35}S-labelled WT- and ΔD1D2-BimEL bound to the indicated GST fusion proteins.

(K) APC^{Cdc20} promotes Bim ubiquitination *in vivo*. IB analysis of WCL and subsequent His-tag pull-down in 8 M urea containing buffer derived from HeLa cells transfected with the indicated plasmids. Cells were pre-treated with 10 μM MG132 for 10 hours to block the proteasome pathway before harvesting.

(L) APC^{Cdc20} promotes Bim ubiquitination *in vitro*. Bacterially expressed and purified WT and ΔD1D2 GST-BimEL proteins were incubated with APC complex purified from M phase HeLa extract together with purified E1, E2 and ubiquitin as indicated at 30° C for 60 minutes before being resolved by SDS-PAGE and probed with the anti-GST antibody.

(M) HCT116 cells were infected with the indicated lentiviral shRNA constructs to generate various Bim expressing stable cell lines. The resulting cell lines were then infected with control or shCdc20 lentiviral constructs to further deplete Cdc20 before harvesting for IB analysis.

(N–O) The cell lines generated in (**M**) were plated for clonogenic survival assays for 14 days with or without challenging with 10 nM Taxol. Crystal violet was used to stain the colonies (**N**) and the colony numbers counted from three independent experiments were presented as mean ± SEM in (**O**).

(P) A schematic illustration of the proposed model for APC^{Cdc20} to interact with Bim and promote its ubiquitination and subsequent degradation in a D-box-dependent manner.

(See also Figure S5)

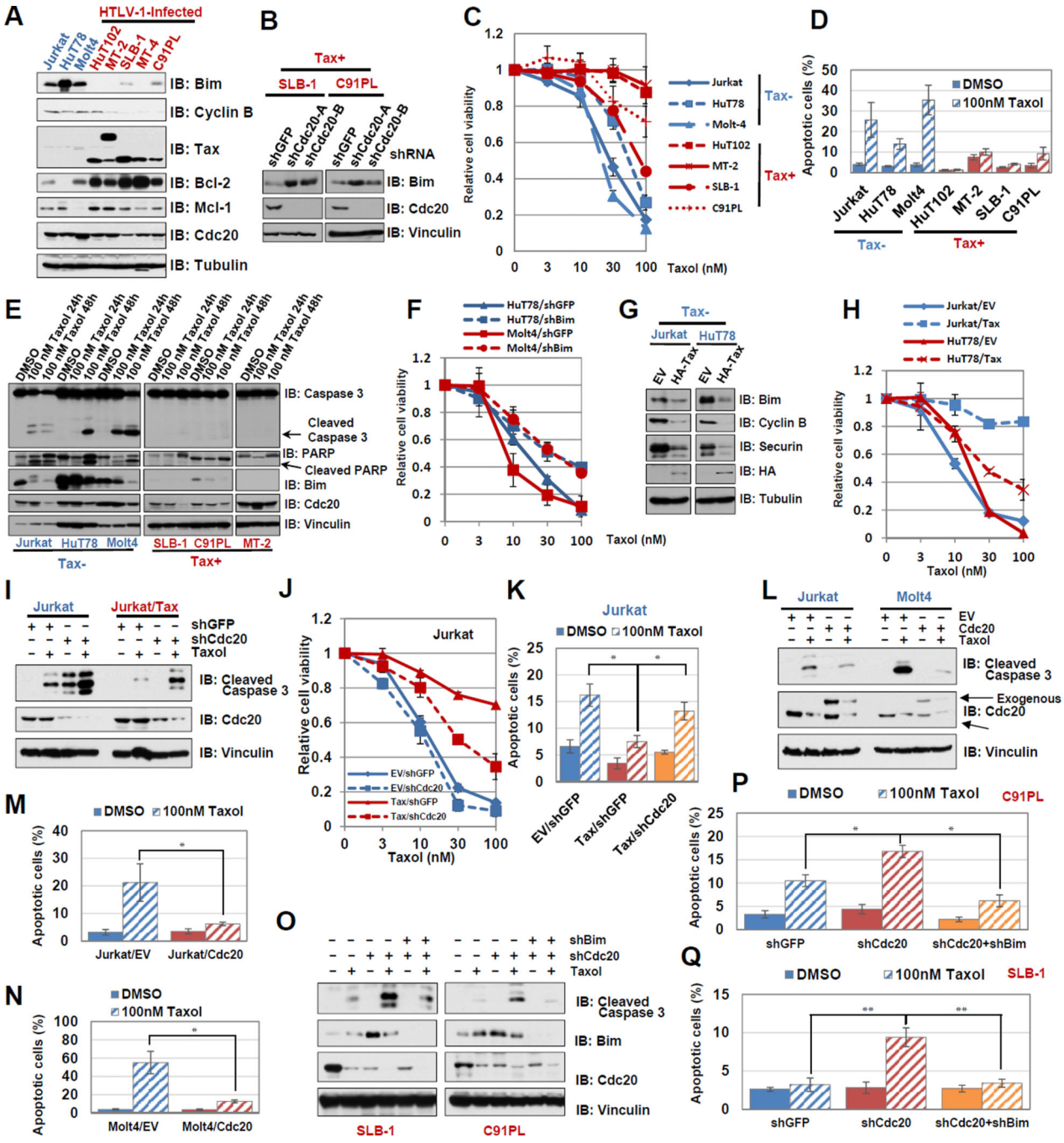

Figure 6. Hyperactive Cdc20 contributes to chemo-resistance through repressing Bim in HTLV-I positive ATL cells

(A) Immunoblot (IB) analysis of whole cell lysates (WCL) derived from various T cell lines.

(B) IB analysis of WCL derived from Tax-positive SLB-1 and C91PL cells infected with the indicated lentiviral shRNA constructs. The infected cells were selected with 1 μg/ml puromycin for 72 hours to eliminate the non-infected cells before harvesting.

(C) Cell viability assays showing that compared to Tax-positive cells, Tax-negative T cell lines were more sensitive to Taxol treatment for 48 hours. Data are shown as mean±SD for three independent experiments.

(D) Quantification of Annexin V and 7-AAD double staining of the indicated cells described in (**C**) after being treated with 100 nM Taxol for 48 hours. Annexin V positively stained cells were considered apoptotic cells. Data are shown as mean±SD for three independent experiments.

(E) IB analysis of WCL derived from T cell lines treated with the indicated doses of Taxol. The cells were harvested at indicated time points for IB analysis.

(F) Cell viability assays showing that compared with shGFP-control cells, Bim-depleted Tax-negative T cell lines HuT78 and Molt4, were more resistant to Taxol treatment for 48 hours. Data are shown as mean±SD for three independent experiments.

(G) IB analysis of WCL derived from Tax-negative Jurkat and HuT78 cells infected with control or Tax-encoding expression retrovirus. The infected cells were selected with 1 μg/ml puromycin for 72 hours to eliminate the non-infected cells before harvesting.

(H) Cell viability assays showing that compared to EV-infected control cells, introducing Tax into Tax-negative T cell lines HuT78 and Jurkat, resulted in acquired resistance to 48 hours Taxol treatment. Data are shown as mean±SD for three independent experiments.

(I) IB analysis of WCL derived from EV and Tax expressing Jurkat cells generated in (**G**) that were further infected with the indicated lentiviral shRNA constructs. The infected cells were selected with 1 μg/ml puromycin for 72 hours to eliminate the non-infected cells and then were treated with 100 nM Taxol for 48 hours before harvesting.

(J) Cell viability assays showing that compared with control cells, Tax expressing Jurkat cells were more sensitive to Cdc20 depletion after being treated with Taxol for 48 hours. Data are shown as mean±SD for three independent experiments.

(K) Quantification of Annexin V and 7-AAD double staining of the indicated cells described in (**J**) after being treated with 100 nM Taxol for 48 hours. Annexin V positively stained cells were considered apoptotic cells. Data are shown as mean±SD for three independent experiments (* $p < 0.05$).

(L) IB analysis of WCL derived from control and Cdc20 expressing Jurkat and Molt4 cells with or without the treatment with 100 nM Taxol for 48 hours.

(M–N) Quantification of Annexin V and 7-AAD double staining of the indicated cells described in (**L**) after being treated with 100 nM Taxol for 48 hours. Annexin V positively stained cells were considered apoptotic cells. Data are shown as mean±SD for three independent experiments (* $p < 0.05$).

(O) IB analysis of WCL derived from Tax positive SLB-1 and C91PL cells infected with the indicated lentiviral shRNA constructs. The infected cells were selected with 1 μg/ml puromycin for 72 hours to eliminate the non-infected cells and then were treated with 100 nM Taxol for 48 hours.

(P–Q) Quantification of Annexin V and 7-AAD double staining of the indicated cells described in (**O**) after being treated with 100 nM Taxol for 48 hours. Annexin V positively stained cells were considered apoptotic cells. Data are shown as mean±SD for three independent experiments (* $p < 0.05$).

(See also Figure S6)

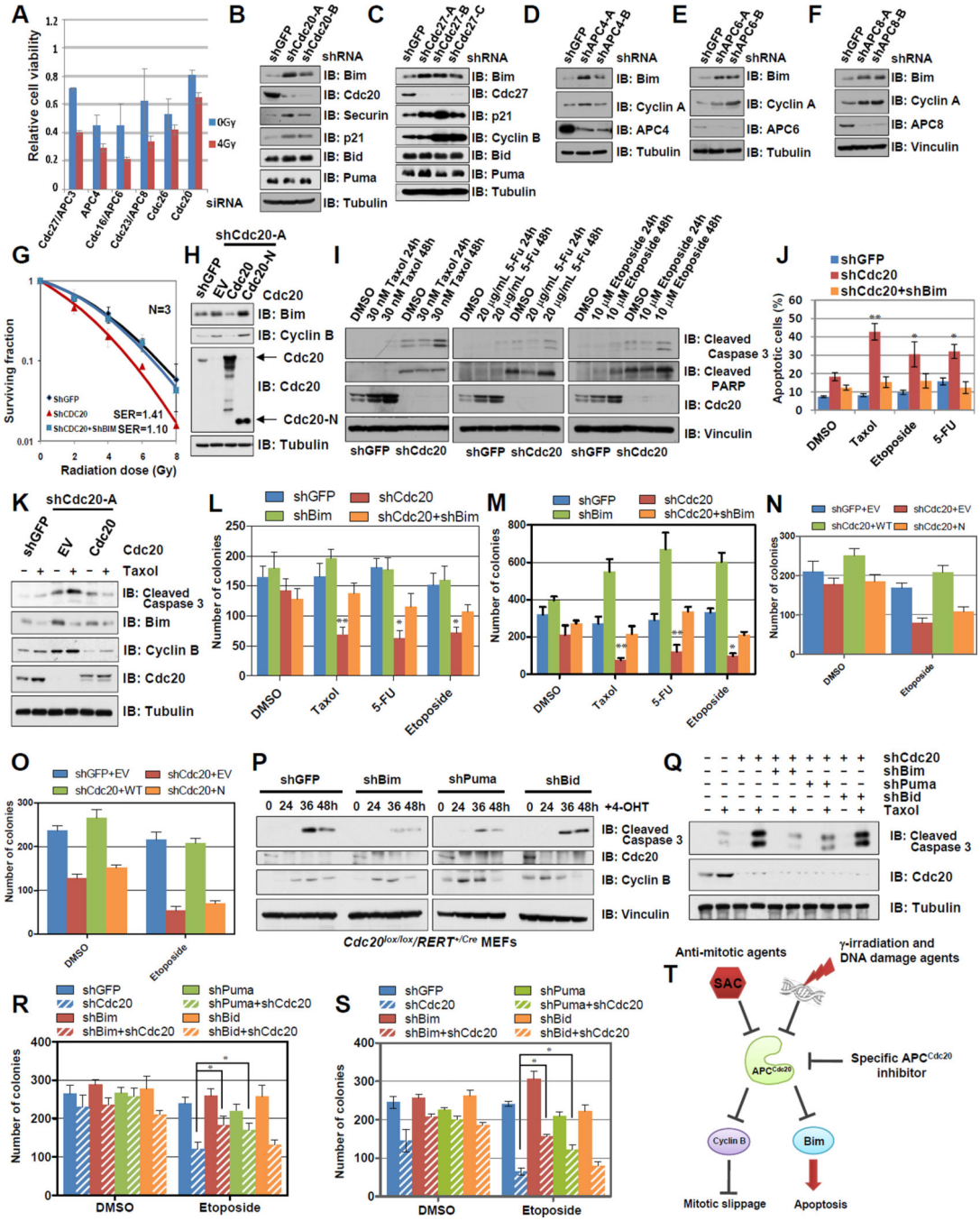

Figure 7. Cdc20 knockdown sensitizes cancer cells to chemo-radiation via Bim accumulation

(A) siRNA screening identified multiple APC^{Cdc20} components as critical regulators of cellular apoptosis in response to γ-irradiation. The relative cell viability of UMSCC-12 cells exposed to 0 Gy and 4 Gy doses of γ-irradiation after siRNA silencing were plotted in relative to the non-silencing control. The data were generated from three independent experiments and shown as mean±SEM (n=3).

(B–F) Immunoblot (IB) analysis of whole cell lysates (WCL) derived from UMSCC-12 cells infected with the indicated lentiviral shRNA constructs. The infected cells were

selected with 1 μg/ml puromycin for 72 hours to eliminate the non-infected cells before harvesting for IB analysis. 10 μM Z-VAD-fmk was added to inhibit caspase-dependent cell death.

(G) UMSCC-12 cells were infected with the indicated lentiviral shRNA constructs for 48 hours, followed by standard clonogenic assays. The data were generated from three independent experiments and shown as mean±SEM (n=3). SER (Sensitization Ehancement Ratio).

(H) IB analysis of UMSCC-12 cells infected with the indicated lentiviral shRNA constructs. The infected cells were selected with 1 μg/ml puromycin for 72 hours to eliminate the non-infected cells before harvesting.

(I) IB analysis of UMSCC-12 cells infected with the indicated lentiviral shRNA constructs. The infected cells were selected with 1 μg/ml puromycin for 72 hours to eliminate the non-infected cells. The resulting cells were further treated with indicated drugs for indicated periods of time before harvesting.

(J) Quantification of Annexin V and 7-AAD double staining of control, Cdc20 knockdown and Bim/Cdc20 double knockdown cells that were treated with or without 30 nM Taxol, 20 μg/mL 5-FU or 10 μM Etoposide for 48 hours. Annexin V positively stained cells were considered apoptotic cells. Data are shown as mean±SD for three independent experiments (** $p < 0.001$, * $p < 0.05$).

(K) IB analysis of UMSCC-12 cells infected with the indicated lentiviral shRNA constructs. The infected cells were selected with 1 μg/ml puromycin for 72 hours to eliminate the non-infected cells. The resulting cells were further treated with 100 nM Taxol for 48 hours before harvesting.

(L) UMSCC-12 cells expressing the indicated shRNA were subjected to clonogenic survival assays for 14 days with or without challenges of various chemotherapeutic reagents (5 nM Taxol, 4 μg/mL 5-FU or 1 μM Etoposide). Crystal violet was used to stain the resulting colonies and the colony numbers were counted from three independent experiments and presented as mean ± SEM (** $p < 0.001$, * $p < 0.05$).

(M) UMSCC-12 cells expressing the indicated shRNA were seeded (3,000 cells per well) in 0.5% low-melting-point agarose in DMEM with 10% FBS, layered onto 0.8% agarose in DMEM/10% FBS. The cells were further treated with or without various chemotherapeutic reagents as indicated (5 nM Taxol, 2 μg/mL 5-FU or 1 μM Etoposide). The plates were cultured for 30 days whereupon the colonies >50 μm were counted under a light microscope. The colony numbers were plotted as mean ± SEM from three independent experiments (** $p < 0.001$, * $p < 0.05$).

(N) UMSCC-12 cells expressing the indicated shRNA were subjected to clonogenic survival assays as described in (**L**). Data were presented as mean±SEM for three independent experiments.

(O) UMSCC-12 cells expressing the indicated shRNA were subjected to soft agar assays as described in (**M**). Data were presented as mean±SEM for three independent experiments.

(P) IB analysis of WCL derived from $Cdc20^{lox/lox}/RERT^{+/Cre}$ MEFs infected with either control, shBim, shPuma or shBid lentiviral shRNA constructs followed by treatment with or without 0.5 μM 4-OHT for 24 hours to induce the depletion of endogenous Cdc20.

(Q) IB analysis of UMSCC-12 cells infected with the indicated lentiviral shRNA constructs. The infected cells were selected with 1 μg/ml puromycin for 72 hours to eliminate the non-

infected cells. The resulting cells were further treated with 100 nM Taxol for 48 hours before harvesting.

(R) UMSCC-12 cells expressing the indicated shRNA were subjected to clonogenic survival assays as described in (**L**). Data were presented as mean±SEM for three independent experiments (* $p < 0.05$).

(S) UMSCC-12 cells expressing indicated shRNAs were subjected to soft agar assays as described in (**M**). Data were presented as mean±SEM for three independent experiments (* $p < 0.05$).

(T) A proposed model for the critical role of the Cdc20-Bim axis in controlling the apoptotic responses to various upstream inputs including anti-mitotic agents and certain DNA damage signals, both of which could inactivate APC^{Cdc20}, leading to the stabilization of Bim and subsequent induction of cellular apoptosis.

(See also Figure S7)